AGU PUBLICATIONS

JGR

Journal of Geophysical Research: Atmospheres

RESEARCH ARTICLE
10.1002/2014JD021487

Key Points:
- Tropical Andean (HDO/H_2O) vapor is lower in austral summer than austral winter
- Air en route to the tropical Andes encounters lower OLR in DJF than JJA
- Upwind monsoon intensity controls tropical Andean DJF (HDO/H_2O) vapor

Correspondence to:
K. E. Samuels-Crow,
samuels@unm.edu

Citation:
Samuels-Crow, K. E., J. Galewsky, D. R. Hardy, Z. D. Sharp, J. Worden, and C. Braun (2014), Upwind convective influences on the isotopic composition of atmospheric water vapor over the tropical Andes, *J. Geophys. Res. Atmos.*, *119*, doi:10.1002/2014JD021487.

Received 10 JAN 2014
Accepted 21 MAY 2014
Accepted article online 27 MAY 2014

Upwind convective influences on the isotopic composition of atmospheric water vapor over the tropical Andes

Kimberly E. Samuels-Crow[1], Joseph Galewsky[1], Douglas R. Hardy[2], Zachary D. Sharp[1], John Worden[3], and Carsten Braun[4]

[1]Department of Earth and Planetary Sciences, University of New Mexico, Albuquerque, New Mexico, USA, [2]Climate System Research Center, University of Massachusetts Amherst, Amherst, Massachusetts, USA, [3]Jet Propulsion Laboratory, California Institute of Technology, Pasadena, California, USA, [4]Geography and Regional Planning/Environmental Science, Westfield State University, Westfield, Massachusetts, USA

Abstract We take advantage of the spatial coverage provided by the Tropospheric Emission Spectrometer on-board the Aura satellite to evaluate processes that control seasonal variations in atmospheric water vapor HDO/H_2O values (δD_{vapor}) over the tropical Andes. δD_{vapor} is lower in austral summer (December, January, and February, DJF) than austral winter (June, July, and August, JJA), which is broadly consistent with precipitation studies and with $\delta^{18}O_{snow}$ preserved in tropical Andean glaciers. In DJF, 64% of δD_{vapor} measurements over the tropical Andes are lower than predicted by Rayleigh distillation while 40% of JJA δD_{vapor} measurements are lower than predicted by Rayleigh distillation. Air that has lower δD_{vapor} than predicted by Rayleigh distillation at a given water vapor concentration (q) encounters low minimum outgoing longwave radiation ($<240\ W\ m^{-2}$) en route to the tropical Andes, suggesting convective intensity controls the isotopic ratios of these measurements. The broad regional coverage of the satellite data allows us to map the spatial extent of the region where isotopic ratios reflect convective processes in different seasons. In DJF, convection strongly influences δD_{vapor} in the central tropical Andes. In JJA, convection influences δD_{vapor} north of the tropical Andes. This pattern suggests that monsoon convection controls δD_{vapor} in austral summer while large-scale advective mixing controls Andean δD_{vapor} in austral winter.

1. Introduction

The seasonal cycle of modern water vapor transport over the tropical Andes is strongly influenced by a complex interplay between the Intertropical Convergence Zone (ITCZ) [*Martínez et al.*, 2011], the strength of the South American monsoon [*Vuille and Werner*, 2005], and the resulting position of the Bolivian High [*Lenters and Cook*, 1999]. Precipitation is strongly seasonal in modern tropical and subtropical South America. During the austral winter, most of South America experiences a dry season with convective precipitation focused north of the equator in the ITCZ [e.g., *Garreaud et al.*, 2008]. In austral summer, a deep continental low-pressure zone forms over the Chaco region of eastern Brazil, feeding convective precipitation associated with the South American Monsoon [e.g., *Garreaud et al.*, 2008] and leading to an upper level high-pressure zone, the Bolivian High [e.g., *Lenters and Cook*, 1999], which is absent in austral winter [e.g., *Garreaud et al.*, 2008]. Easterly winds associated with the Bolivian High transport moisture to the Altiplano and lead to the development of deep convection in the Andes during austral summer [e.g., *Garreaud et al.*, 2003, 2008]. Researchers have used paleoclimate proxies preserved in ice cores from Quelccaya Ice Cap [e.g., *Grootes et al.*, 1989; *Thompson et al.*, 2013], Huascaran [e.g., *Thompson et al.*, 1995; *Broecker*, 1997; *Pierrehumbert*, 1999], Illimani [e.g., *Ramirez et al.*, 2003; *Hoffmann et al.*, 2003], and Chimborazo [e.g., *Vimeux et al.*, 2009] (Figure 1) to reconstruct past tropical climate variability and from Sajama [e.g., *Thompson et al.*, 2000] to reconstruct past climate variability in the northern subtropics [*Kaser and Osmaston*, 2002]. However, the interpretation of the oxygen isotope ratios in the ice ($\delta^{18}O_{snow}$) [e.g., *Thompson et al.*, 2013] remains challenging.

Seasonal variations in observed tropical Andean $\delta^{18}O_{snow}$ are the central issue. Whereas there is a positive correlation between air temperature and $\delta^{18}O_{snow}$ in polar ice (isotope temperature effect) [*Dansgaard*, 1964], tropical Andean $\delta^{18}O_{snow}$ is lower in the austral summer (DJF) than in the austral winter (JJA) despite relatively uniform annual temperatures [*Thompson*, 2000]. Many researchers have concluded that regional $\delta^{18}O_{snow}$ preserves information about upwind precipitation history [e.g., *Hoffmann et al.*, 2003; *Vuille et al.*,

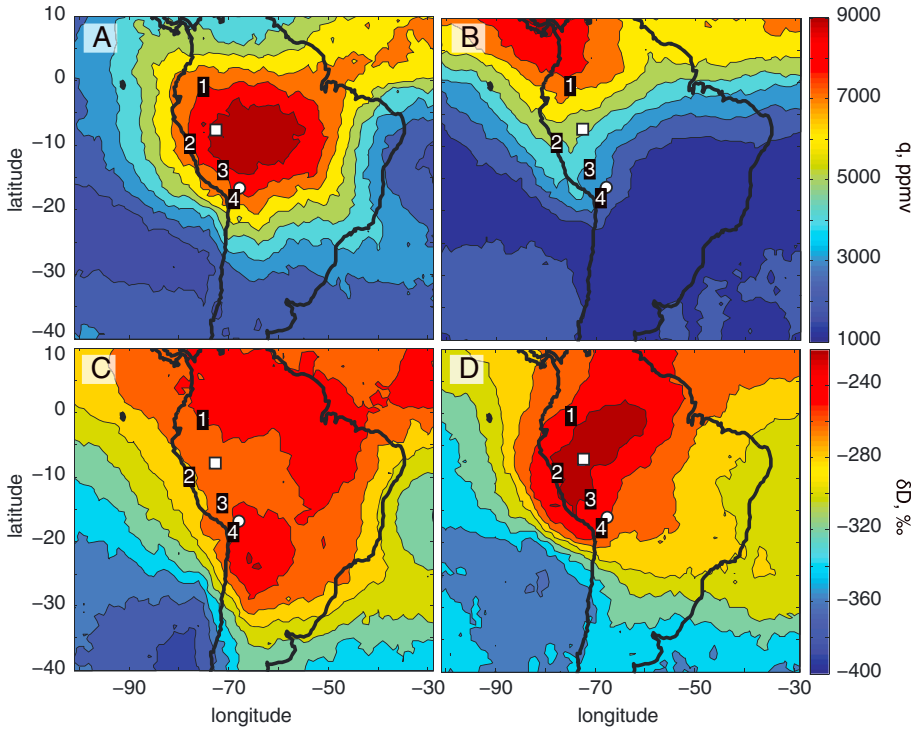

Figure 1. Maps of South America showing TES water vapor concentration for (a) DJF and (b) JJA along with TES δD for (c) DJF and (d) JJA. Filled rectangles denote the locations of ice caps in the (1) northern tropical Andes (Chimborazo), (2) central tropical Andes (Huascaran), (3) southern tropical Andes (Quelccaya), and (4) northern subtropics (Sajama). The white square shows the location of the Cruzeiro do Sul sounding data. The white circle shows the location of Illimani ice cap.

2003a, 2003b; *Vimeux et al.*, 2005; *Vuille and Werner*, 2005; *Sturm et al.*, 2007; *Villacís et al.*, 2008; *Vimeux et al.*, 2011] instead of temperature [*Thompson et al.*, 2003], suggesting that the "isotope amount effect" [*Dansgaard*, 1964] primarily controls the isotopic composition of tropical ice.

Isotopic ratios in precipitation from valleys adjacent to Chimborazo [*Villacís et al.*, 2008] and Cerro El Consuelo [*Windhorst et al.*, 2013] in Ecuador and Illimani in Bolivia [*Vimeux et al.*, 2005] have been linked to upwind, rather than local, processes, but the data are spatially and temporally limited. Joint measurements of atmospheric water vapor concentration (q) and hydrogen isotope ratios (δD_{vapor}) may constrain the relative importance of large-scale advective mixing and convective processes in different seasons throughout the region [*Worden et al.*, 2007; *Noone*, 2012]. The joint distribution of δD_{vapor} and q has been used to distinguish between processes that transport water vapor through the tropics [*Worden et al.*, 2007] and to the subtropics [e.g., *Risi et al.*, 2010; *Galewsky et al.*, 2011] and monsoon regions [*Brown et al.*, 2008]. Other studies have used the joint distribution of q and δD_{vapor} to quantify convective processes, including entrainment of vapor from the unsaturated downdraft into the subcloud layer, that govern observed decreases in isotopic ratios with increased precipitation [*Risi et al.*, 2008].

The goal of this study is to use satellite measurements from NASA's Tropospheric Emission Spectrometer (TES) to determine seasonal variability in δD_{vapor} over the tropical Andes and to explore the links between modern δD_{vapor} and upwind convective intensity. Satellite data provide spatial coverage impossible to achieve in ground-based studies, allowing us to evaluate how processes change from north to south along the spine of the Andes and through the region affected by the South American summer monsoon [*Zhou and Lau*, 1998], when most of the accumulation takes place on the tropical glaciers [e.g., *Vuille et al.*, 2000; *Hardy et al.*, 2003]. Many processes are involved in the conversion of atmospheric water vapor to glacial ice, including postdepositional processes such as wind scour, sublimation, and melting, in this topographically complex region [e.g., *Hardy*, 2003]. Our goal is to advance our knowledge of modern water vapor dynamics in the tropical Andes, which may provide insights into past processes preserved in the ice core record and to map out the regions of South America where isotopic ratios in water vapor are affected by convection in different seasons.

2. Methods

2.1. Satellite Measurements of Isotopic Ratios

Water isotopologues (HDO, $H_2{}^{16}O$, and $H_2{}^{18}O$) fractionate during phase changes with evaporation and condensation concentrating the heavier isotopologues in the liquid. We can, therefore, use isotopic ratios in water vapor to trace atmospheric processes, including Rayleigh distillation, subcloud raindrop evaporation, diffusion, and large-scale mixing [*Worden et al.*, 2006; *Galewsky and Hurley*, 2010; *Noone*, 2012]. HDO/H_2O ratios are reported as the per mil (‰) difference (δ) between the isotopic ratio of the sample (R_{sample}) and standard (R_{std}), in this case standard mean ocean water (SMOW): $\delta D = 1000(R_{sample}/R_{std} - 1)$.

TES, aboard NASA's Aura satellite launched in 2004, provides near-global measurements of infrared radiation from Earth's surface and atmospheric gases, including H_2O and HDO. TES is a Fourier transform spectrometer that measures infrared radiation from 650 cm^{-1} to 3050 cm^{-1} in limb and nadir mode [*Worden et al.*, 2006; *Noone*, 2012]. We used Level 2 nadir measurements from the TES Lite v006 data set to calculate seasonal and monthly averages of δD_{vapor} ($\overline{\delta D}_{vapor}$) and q ($\bar{q}$) over 10° × 10° boxes centered around Chimborazo (0.9°S, 74.5°W) (northern tropical Andes), Huascaran (9°S, 78°W) (central tropical Andes), Quelccaya Ice Cap (14°S, 71°W) (southern tropical Andes), and Sajama (18°S, 69°W) (northern subtropical Andes) at 510.9 hPa, and over a broad region of South America that incorporates the tropical and northern subtropical Andes (Figure 1). TES nadir measurements have a ground footprint of 5.3 km × 8.3 km. TES Lite data are bias corrected for known problems in HDO measurements and have greater vertical resolution than previous versions of the TES data [*Worden et al.*, 2012] and other satellite instruments [e.g., *Lacour et al.*, 2012], allowing us to distinguish between the boundary layer and free troposphere. The TES data have peak sensitivity ~500 hPa, and averaging kernels strongly overlap at this level [*Worden et al.*, 2012], so free troposphere measurements require no further correction and a single level can be used rather than a weighted average in the vertical.

To ensure high data quality, we used TES measurements from 2004 to 2011 with degrees of freedom for signal (DOFS) > 0.7 in the free troposphere and a retrieval quality flag of 1. We determined DOFS in the free troposphere by summing the averaging kernel diagonal for HDO from 750 to 100 hPa. Mean DOFS was greater than 1 in each domain and each season and differed by less than 0.1 between seasons in each domain. At Quelccaya Ice Cap, 763 December, January, and February (DJF) and 772 June, July, and August (JJA) measurements meet these criteria. At Chimborazo, 830 and 795 measurements met these criteria for DJF and JJA respectively. At Huascaran, 777 and 723 measurements met these criteria for DJF and JJA, respectively, and, at Sajama, 716 and 564 measurements met these criteria for DJF and JJA, respectively. On average, these measurements occurred every 3.9 days within each 10° × 10° domain and include more than half of the TES measurements in the study area. The broader tropical Andean region shown in Figure 1 incorporates more than 20,000 measurements in both DJF and JJA. Mean degrees of freedom for signal, the primary means to quantify the sensitivity of TES retrievals to a number of factors, including clouds, shows little seasonal variation in the domains described above. Therefore, variations in interferences have little impact on seasonal variability in δD_{vapor} measurements [e.g., *Worden et al.*, 2007; *Lee et al.*, 2011].

2.2. Ground-Based Sample Collection

We collected eleven air samples at the summit of Quelccaya Ice Cap in evacuated glass flasks [*Strong et al.*, 2007] from 7 to 9 July 2011. Local conditions were measured simultaneously with a handheld Kestrel weather meter and an automated weather station installed at the summit of the ice cap in August 2003 [e.g., *Hardy and Hardy*, 2008; *Bradley et al.*, 2009; *Hardy*, 2011]. The average atmospheric pressure at the summit of Quelccaya Ice Cap during the sampling period was 512 hPa, making these samples directly comparable to the TES measurements. We cryogenically isolated the water vapor in the University of New Mexico's stable isotope lab following methods described by *Strong et al.* [2007] and *Johnson et al.* [2011] and converted the water vapor to H_2 gas using a zinc reduction method [*Friedman*, 1953]. We then determined the δD of the H_2 gas on a Finnegan MAT-252 mass spectrometer at the University of New Mexico. Small sample size precluded $\delta^{18}O_{vapor}$ measurements.

2.3. Theoretical Curves

The Rayleigh model, which describes progressive, open-system isotopic change, is a first-order tool for diagnosing processes that control δD_{vapor} and q. The Rayleigh model assumes the condensed water vapor is completely removed from the system, decreasing the isotopic ratios of the remaining vapor. This process

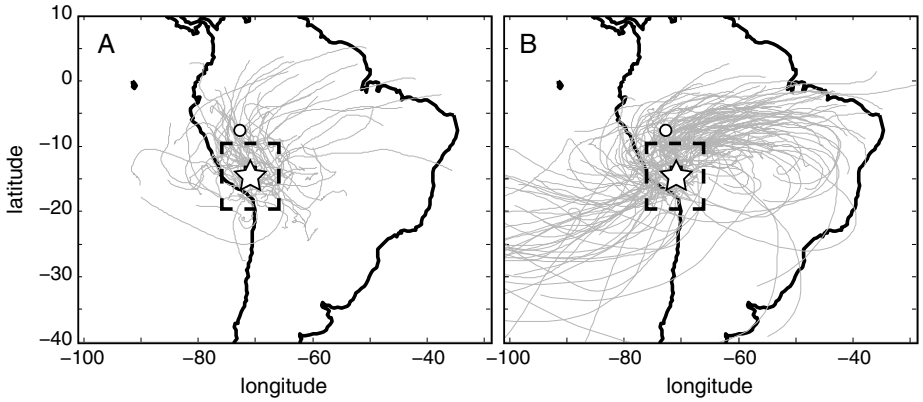

Figure 2. Maps of sample back trajectories launched from the southern tropical Andes (Quelccaya) in (a) DJF and (b) JJA. The glacier at the center of the domain is shown with a white star. The heavy dashed line shows the boundary of the 10° × 10° domain. The white circle shows the location of Cruzeiro do Sul.

results in decreased δD_{vapor} with decreased q, decreased temperature, increased elevation, and increased distance from the source region [e.g., *Dansgaard*, 1964; *Gat*, 1996]. Deviations from the Rayleigh model can provide insights into other processes that contribute to the isotopic composition of water vapor in the tropics and monsoon regions [e.g., *Brown et al.*, 2008]. δD_{vapor} that falls below the Rayleigh curve is generally associated with moisture recycling in convective clouds while δD_{vapor} that falls above the Rayleigh curve is typically associated with advective mixing [e.g., *Worden et al.*, 2007; *Noone*, 2012].

We calculated Rayleigh curves as a function of q at saturation based on vertical temperature profiles from atmospheric soundings at Cruzeiro do Sul, Brazil (http://weather.uwyo.edu/upperair/sounding.html), which is upwind of the central and southern tropical Andean glaciers (Figure 1), based on the equation $d\ln R = (\alpha - 1)\, d\ln q$ where R is the D/H ratio, α is the temperature-dependent fractionation factor, and q is the water vapor mixing ratio [e.g., *Dessler and Sherwood*, 2003]. We calculated mixing curves based on the equation:

$$\delta D_{mix} = 1000\left[\left(\frac{f[D]_1+(1-f)[D]_2}{f[H]_1+(1-f)[H]_2}\Big/\left(\frac{D}{H}\right)_{VSMOW}\right)-1\right]$$

where f is the mixing fraction [e.g., *Gedzelman*, 1988; *Dessler and Sherwood*, 2003].

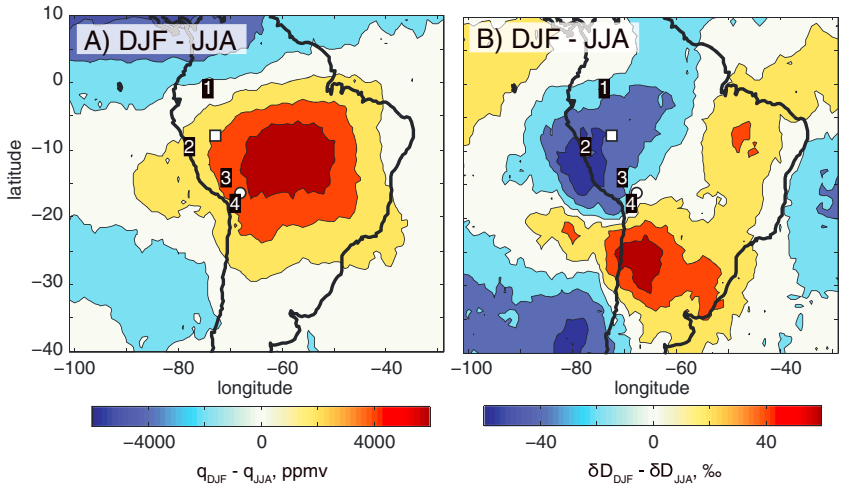

Figure 3. Maps of South America showing seasonal differences in TES (a) q and (b) δD_{vapor} ($\delta D_{DJF} - \delta D_{JJA}$) with the locations of tropical ice caps (filled rectangles) in the (1) northern tropical (Chimborazo), (2) central tropical (Huascaran), (3) southern tropical (Quelccaya), and (4) northern subtropical (Sajama) Andes and the site of Cruzeiro do Sul sounding data (circle) shown.

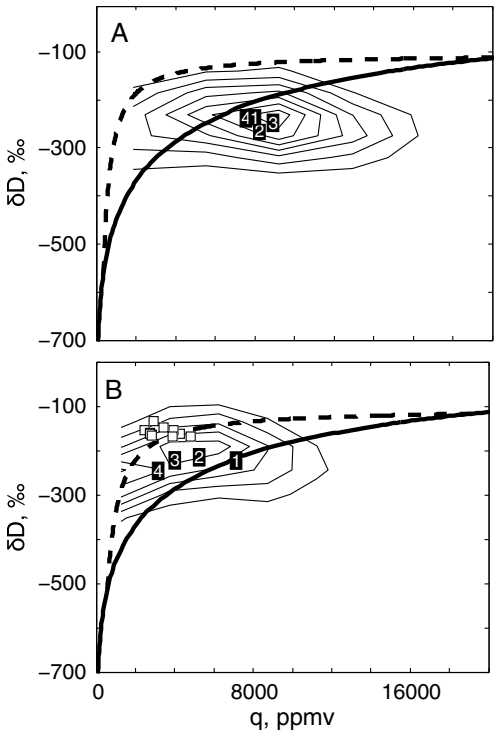

Figure 4. Two-dimensional histograms (light solid lines) of TES δD_{vapor} and q in the tropical and northern subtropical Andean glacier region in (a) DJF and (b) JJA with Quelccaya Ice Cap (QIC) flask measurements from 2011 (white squares). The contours indicate the frequency of TES measurements with a particular δD and q, and the contour interval for the TES data is number of measurements = 50. Filled rectangles indicate the mean seasonal values for 10° × 10° domains centered on the (1) northern tropical, (2) central tropical, (3) southern tropical, and (4) northern subtropical Andes. The heavy lines are the calculated Rayleigh (solid line) and mixing (dashed line) curves. The Rayleigh curve was calculated with $\delta D_{initial} = -90‰$ and $q_{initial} = 26479$ ppmv. The mixing curve was calculated using a wet end-member with $\delta D = -86‰$ and $q = 19162$ ppmv and a dry end-member with $\delta D = -496‰$ and $q = 574$ ppmv.

In order to calculate the Rayleigh curve, we used an initial δD_{vapor} of −90‰, consistent with δD_{vapor} in equilibrium with the tropical Atlantic [*Craig and Gordon*, 1965] and an initial q of 26479 ppmv, consistent with the saturation vapor pressure at low elevations over Cruzeiro do Sul. We used fractionation factors of *Majoube* [1971] for fractionation between liquid and vapor above 0°C and *Merlivat and Nief* [1967] for fractionation between solid and vapor at temperatures below 0°C. We tested the sensitivity of the Rayleigh curve calculations to choice of sounding data by comparing Rayleigh curves calculated from Cruzeiro do Sul sounding data to Rayleigh curves calculated based on soundings from locations in the Amazon Basin, but these calculations did not yield significantly different results.

In order to determine how the measured δD_{vapor} deviates from the Rayleigh prediction at the given q, we subtracted the measured δD_{vapor} from the Rayleigh prediction at the given $q \pm 100$ ppmv: $\Delta\delta D = \delta D_{Rayleigh} - \delta D_{TES}$. When a measurement lies on the Rayleigh curve (i.e., $\Delta\delta D = 0‰$) open-system equilibrium fractionation controls the isotopic composition of the water vapor. Measurements that lie above the Rayleigh curve have a $\Delta\delta D < 0‰$, suggesting that advective mixing between moist air with relatively high δD and dry air with relatively low δD controls the isotopic composition of the water vapor. Measurements that fall below the Rayleigh curve have a $\Delta\delta D > 0‰$ and are associated with convective moisture recycling, whereby the vapor and liquid coexist after condensation and entrainment of low δD water vapor from unsaturated downdrafts decreases the isotopic ratios in the convective system [e.g., *Risi et al.*, 2008].

2.4. Lagrangian Back Trajectories and Outgoing Longwave Radiation

We investigated links between δD_{vapor} and convective intensity by determining the minimum outgoing longwave radiation (OLR) along back trajectories upwind of each TES measurement. Low OLR is primarily controlled by high cirrus clouds, which are produced by deep convection and cannot persist long term without convective conditions [*Zhang*, 1993]. Therefore, low OLR is often used to identify intense tropical convection and the onset of monsoon precipitation in monsoon regions [e.g., *Kousky*, 1988; *Kousky and Kayano*, 1994; *Moron*, 1995; *Singh*, 2005; *Vuille and Werner*, 2005; *Susskind et al.*, 2012]. In Amazonia, a seasonal average OLR of 240 W m^{-2} or lower is considered diagnostic of the South American monsoon [*Kousky*, 1988]. Average AIRS cloud top temperatures in the study region are ~255 K, suggesting that cirrus clouds fed by deep convection likely control OLR encountered along trajectories [*Zhang*, 1993] and confirming that low OLR can be used as a proxy for regional convection.

In order to determine the minimum OLR air encounters en route to the tropical Andes, we first calculated 5-day Lagrangian back trajectories from each TES measurement using NOAA's Hybrid Single-Particle Lagrangian Integrated Trajectory (HYSPLIT) model driven by National Centers for Environmental Prediction-National Center for Atmospheric Research Reanalysis data [*Draxler and Hess*, 1997]. Vertical motion is based on vertical velocity fields from the reanalysis data set [*Draxler and Hess*, 1997; *Draxler*, 1999]. Sample trajectories are shown in Figure 2.

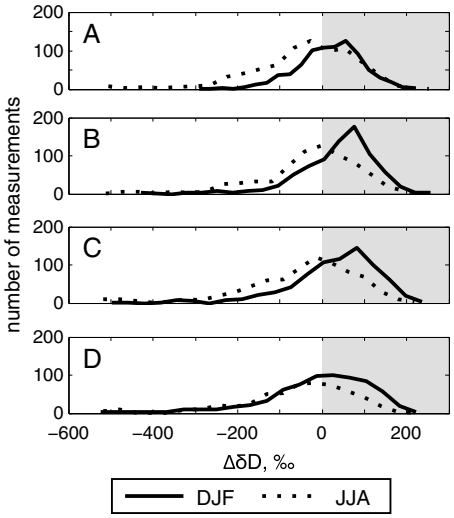

Figure 5. Histograms showing the variability of $\Delta\delta D$ ($\Delta\delta D = \delta D_{\text{Rayleigh}} - \delta D_{\text{TES}}$) in the (a) northern tropical, (b) central tropical, (c) southern tropical, and (d) northern subtropical Andes in DJF (solid lines) and JJA (dashed lines). Shaded region indicates that $\Delta\delta D$ is positive.

In order to determine the sensitivity of the trajectory location to vertical motion in this highly convective and topographically complex region, we launched a subset of trajectories from 1000 m above TES measurements in 10° × 10° domains above Quelccaya Ice Cap in the tropical Andes (13.9°S, 70.8°W), eastern Brazil (10.2°S, 40.8°W), and the Pacific (14°S, 90°W) and compared the location of the trajectory launched from the TES measurement to the trajectory launched 1000 m above the TES measurement. Additionally, we calculated a subset of the trajectories using the Global Data Assimilation System (GDAS1) to test the sensitivity of HYSPLIT to variations in meteorological input.

Once back trajectories were calculated for each TES measurement, we used daily level 3 OLR data from the Atmospheric Infrared Sounder (AIRS) version 6 to determine the OLR within a 2° × 2° domain around each trajectory 24, 48, 72, 96, and 120 h before the TES measurement. OLR data from the AIRS instrument are consistent with OLR data from the Clouds and Earth's Radiant Energy System data and have been used to link variability in tropical OLR with the El Niño–Southern Oscillation Index [*Susskind et al.*, 2012]. We determined the minimum OLR along each 5 day trajectory as a proxy for maximum convective intensity. In order to evaluate the influence of local convection, we determined average OLR on the day of each TES measurement and the average difference, both spatially and temporally, between the TES measurement and minimum OLR.

Despite the discrepancies in the precise locations of trajectories calculated based on different meteorological input and between trajectories launched at different elevations, each trajectory encountered minimum OLR in the same region (not shown), and minimum OLR encountered along trajectories was consistent. Mean minimum OLR along back trajectories launched from the elevation of the TES measurement and from 1000 m above the TES measurement varied by only 2 W m^{-2} at Quelccaya Ice Cap, 4 W m^{-2} over the Pacific, and 10 W m^{-2} over eastern Brazil. In DJF, OLR along the subset of trajectories driven by GDAS1 was, on average, 7 W m^{-2} higher than OLR along trajectories driven by the Reanalysis data set. In JJA, OLR along the subset of trajectories driven by GDAS1 was, on average, 2 W m^{-2} higher than OLR along trajectories driven by the Reanalysis data set.

3. Results

3.1. Seasonal δD and q Variations

Seasonal variations in q are consistent with precipitation patterns in tropical South America [e.g., *Garreaud et al.*, 2008]. During the austral summer, q is highest over Brazil (Figure 1a) while q is highest in the vicinity of the equator in austral winter (Figure 1b). δD_{vapor} does not follow the same spatial pattern as q in austral summer (Figure 1c) or austral winter (Figure 1d). Seasonal $\overline{\delta D}_{\text{vapor}}$ in the tropical Andes is lower in DJF (Figure 3a) when q is higher than it is in JJA (Figure 3b). This seasonal pattern is broadly consistent with seasonal variations in tropical Andean precipitation [e.g., *Vimeux et al.*, 2005] and $\delta^{18}O_{\text{snow}}$ [*Thompson*, 2000] but is inconsistent with Rayleigh distillation based on starting δD_{vapor} and q consistent with a tropical source region. Seasonal $\overline{\delta D}_{\text{vapor}}$ in DJF is lower in the central tropical Andes (−260‰), than in the northern tropical Andes (−238‰), southern tropical Andes (−247‰), or the northern subtropical Andes (−236‰). In JJA, $\overline{\delta D}_{\text{vapor}}$ is 14‰ to 33‰ higher than it is in DJF while $\overline{\delta D}_{\text{vapor}}$ in the northern subtropical Andes is 4‰ lower than in DJF (Figure 4).

In the tropical Andes, 67% to 73% of the DJF TES measurements fall below the Rayleigh curve (i.e., $\Delta\delta D > 0$‰) with the highest proportion of measurements below the Rayleigh curve in the central tropical Andes. In the

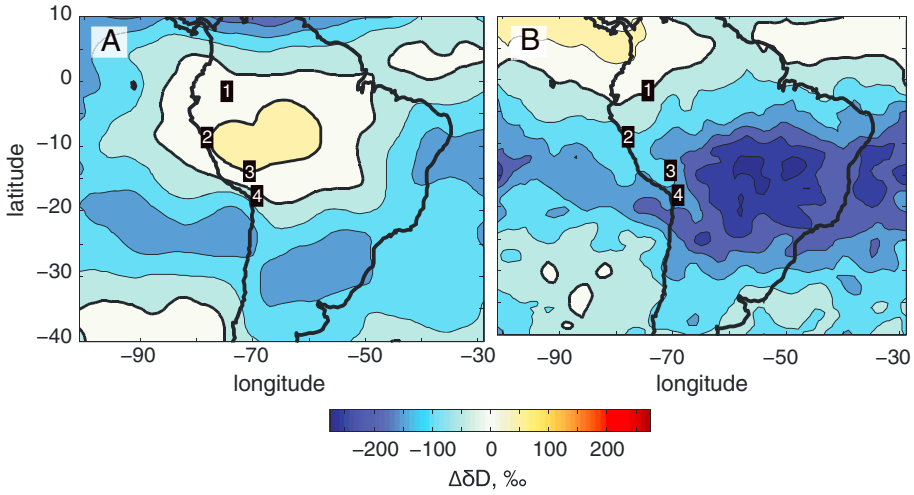

Figure 6. Maps of $\Delta\delta D$ ($\Delta\delta D = \delta D_{\text{Rayleigh}} - \delta D_{\text{TES}}$) for (a) DJF and (b) JJA. Measurements that fall below the Rayleigh curve (i.e., $\Delta\delta D > 0$‰) are designated by solid lines while measurements that lie above the Rayleigh curve are designated by dashed lines. The zero contour is drawn with a heavy solid line. In DJF, measurements with $\Delta\delta D > 0$‰ are centered over the tropical Andes and upper Amazon Basin. In JJA, measurements with $\Delta\delta D > 0$‰ are located north of the tropical Andes. Filled rectangles indicate the locations of glaciers included in the study as in Figures 1 and 3. The contour interval is $\Delta\delta D = 20$‰.

northern subtropical Andes, 52% of the DJF TES measurements fall below the Rayleigh curve. DJF average $\Delta\delta D_{\text{vapor}}$ is +18‰ to 28‰ in the northern and southern tropical Andes and +36‰ in the central tropical Andes. In contrast, in the northern subtropical Andes, average $\Delta\delta D$ is −12‰ (Figure 5). Spatially, the region where $\Delta\delta D > 0$‰ in DJF forms a bull's eye that extends from around 65°W to 95°W and the equator to 20°S (Figure 6a).

While DJF $\Delta\delta D$ is positive in the tropical Andes, JJA δD_{vapor} is higher than predicted by the Rayleigh model (i.e., $\Delta\delta D < 0$‰). JJA $\Delta\delta D$ ranges from −142‰ in the northern subtropical Andes to −6‰ in the northern tropical Andes (Figure 6b). This is consistent with water vapor sampled at the summit of Quelccaya Ice Cap in July 2011, which has an average $\Delta\delta D_{\text{vapor}}$ of −148‰ (Table 1). Whereas DJF $\Delta\delta D$ is highest in the central tropical Andes, there is a linear relationship ($r = 0.994$, $p = 0.0057997$) between latitude and mean $\Delta\delta D$ along the spine of the Andes in JJA, and the region where $\Delta\delta D > 0$‰ shifts north of the equator (Figure 6b). This spatial difference in $\Delta\delta D$ suggests that the dominant processes controlling the isotopic composition of water vapor over the tropical Andean glaciers differ seasonally.

3.2. Upwind Convective Intensity

More than half (64%) of the DJF and 40% of the JJA δD_{vapor} measurements in the tropical and northern subtropical Andes have $\Delta\delta D > 0$‰, consistent with an interpretation that the air parcels have undergone

Table 1. δD_{vapor}, q, and Local Conditions for Quelccaya Ice Cap Flask Samples

Date	Time[a]	T (°C)	T_d (°C)	q (ppmv)	δD_{vapor} (‰)	$\Delta\delta D$ (‰)
7/7/11	1300	−6.5	−16.1	2940	−134	−183
7/7/11	1852	−9.5	−18.0	2460	−153	−185
7/8/11	0700	−9.5	−16.5	2830	−164	−158
7/8/11	1300	−7.1	−12.0	4280	−162	−111
7/8/11	1600	−7.0	−12.9	3940	−155	−129
7/8/11	1900	−9.5	−14.4	3440	−148	−151
7/9/11	0100	−10.0	−16.8	2750	−161	−164
7/9/11	0100[2]	−10.0	−16.8	2750	−161	−164
7/9/11	0540	−10.5	−13.1	3870	−168	−118
7/9/11	0700	−10.6	−10.7	4810	−168	−91
7/9/11	1300	−4.3	−16.4	2860	−166	−155

[a]Duplicate sample, T = temperature, T_d = Dewpoint, q = water vapor concentration. Dates are formatted as month/day/year.
[b]Local time (UTC/GMT − 5 h).

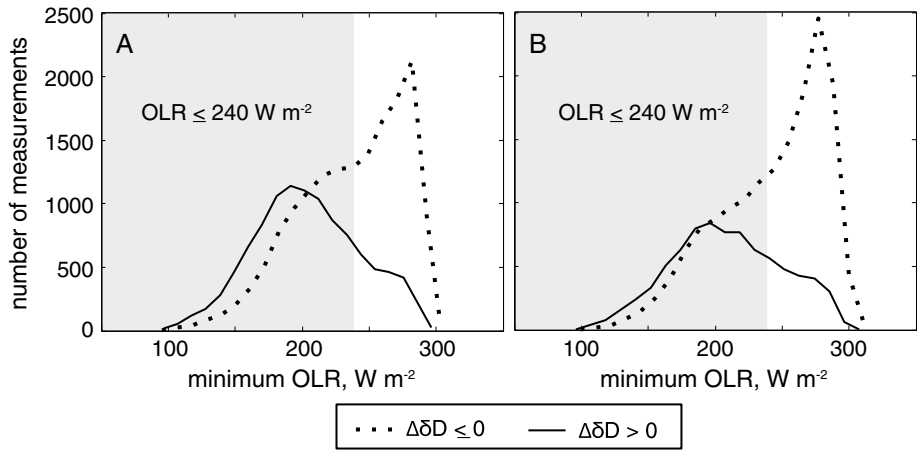

Figure 7. Histograms of minimum OLR encountered en route to the tropical Andes show that minimum OLR along trajectories is lower for measurements with $\Delta\delta D > 0‰$ (solid lines) than for measurements with $\Delta\delta D < 0‰$ (dashed lines) in both (a) DJF and (b) JJA. OLR $< 240\ W\ m^{-2}$ (gray field) is diagnostic of periods of intense convection in tropical South America.

intense convection [*Worden et al.*, 2007; *Noone*, 2012]. The goal of this section is to explicitly evaluate the link between TES measurements with $\Delta\delta D > 0‰$ and proxies of upwind convective intensity.

Five day back trajectories indicate that air parcels with $\Delta\delta D > 0‰$ travel through regions with mean minimum OLR $< 240\ W\ m^{-2}$ (Figure 7). Air parcels with $\Delta\delta D < 0‰$ encounter higher average minimum OLR prior to arriving in the tropical Andes. Histograms of minimum OLR along trajectories show that in DJF (Figure 7a) mean minimum OLR along all trajectories is $224\ W\ m^{-2}$. This is consistent with intense convection throughout the region during the monsoon season. DJF measurements with $\Delta\delta D > 0‰$ encounter lower average minimum OLR along trajectories ($204\ W\ m^{-2}$) than DJF measurements with $\Delta\delta D < 0‰$ ($237\ W\ m^{-2}$) (Figure 7a). In JJA (Figure 7b), average minimum OLR along all trajectories is $228\ W\ m^{-2}$. JJA measurements with $\Delta\delta D > 0‰$ also encounter lower average minimum OLR ($209\ W\ m^{-2}$) than other JJA measurements ($243\ W\ m^{-2}$) (Figure 7b).

Contour maps of minimum OLR encountered along air parcel trajectories show that, in austral summer, air encounters the lowest OLR en route to the central tropical Andes and to the east of the central tropical Andes (Figure 8a). Spatially, this relationship forms a bull's eye with a minimum OLR $< 200\ W\ m^{-2}$ that extends from around 50°W to 80°W and 20°S to 5°N (Figure 6a). In austral winter, air passes through regions with OLR $< 200\ W\ m^{-2}$ en route to the area between the equator and the northern tropical Andes (Figure 8b). In contrast, the central and southern tropical and northern subtropical Andes are influenced by upwind

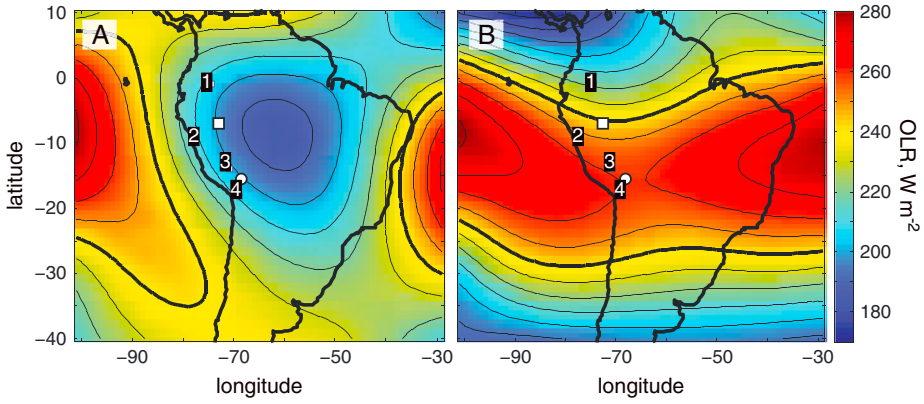

Figure 8. Contour maps of minimum OLR encountered along back trajectories upwind of each TES δD measurement in (a) DJF and (b) JJA. Trajectories launched from measurements with the highest $\Delta\delta D$ (see Figure 6) encountered OLR $< 200\ W\ m^{-2}$ in DJF and JJA. Filled rectangles indicate the locations of glaciers included in the study as in Figures 1 and 3. The contour interval is $20\ W\ m^{-2}$.

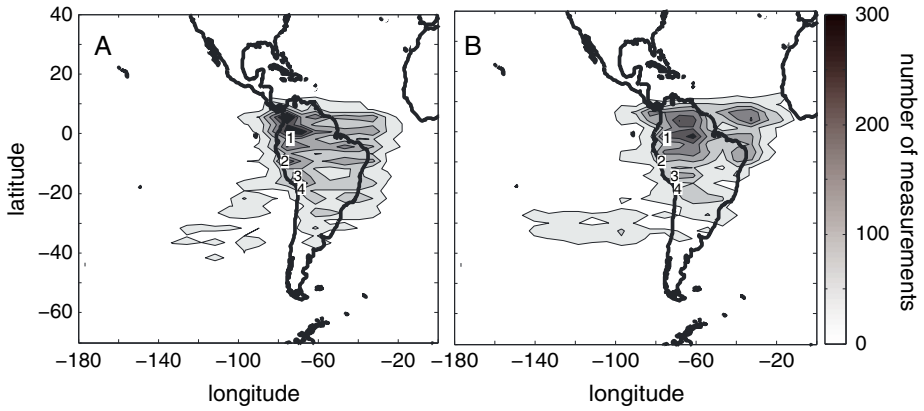

Figure 9. Two-dimensional histograms showing the locations where minimum OLR was encountered along trajectories in (a) DJF and (b) JJA. The gray scale indicates the number of trajectories that encountered minimum OLR at each location. Filled rectangles indicate the locations of glaciers included in the study as in Figures 1 and 3.

OLR $> 240\,\mathrm{W\,m^{-2}}$ in JJA (Figure 6b). Maps that show the probability density function of the location where minimum OLR was encountered en route to the $10° \times 10°$ domains around each glacier show that minimum OLR in DJF (Figure 9a) was encountered slightly further south and west of where it was encountered in JJA (Figure 9b).

Local convection appears to exert only a minor influence over $\delta D_{\mathrm{vapor}}$ measured in the tropical Andes (Figure 10). Regardless of season, less than 1% of the back trajectories launched from each TES measurement encountered OLR the day the trajectory was launched (Figures 10a and 10b). In DJF, the average distance

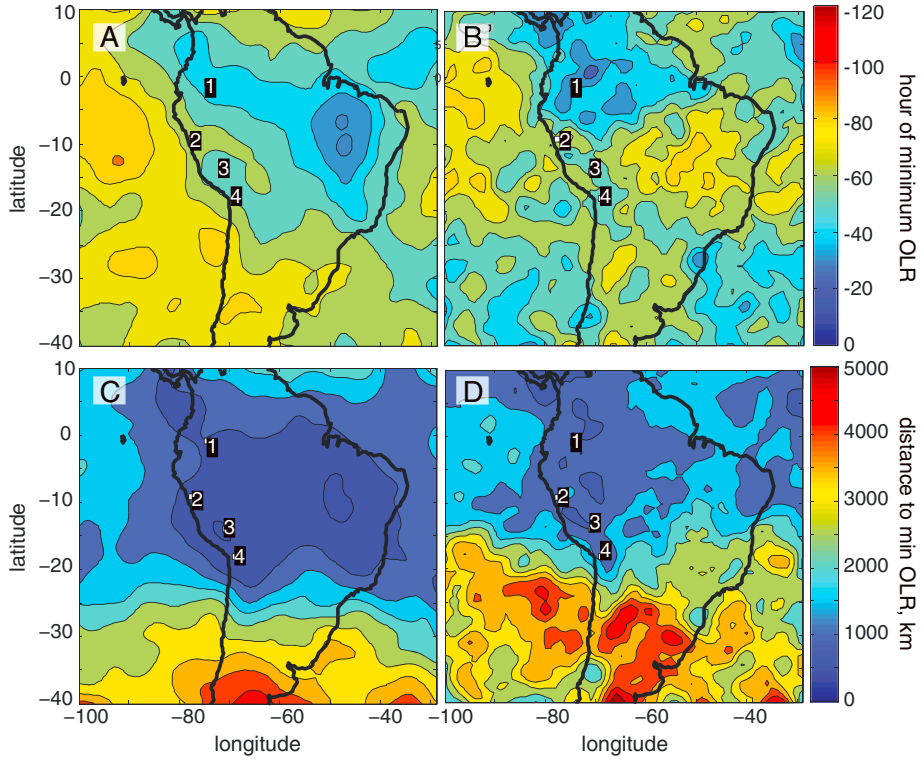

Figure 10. Maps showing the difference between the time of the TES measurement and minimum OLR for (a) DJF and (b) JJA along with maps of the distance between the location of the TES measurement and the minimum OLR encountered along trajectories in (c) DJF and (d) JJA. This analysis shows that the δD measured by the TES instrument is typically the product of upwind, rather than local, processes.

between the measurement location and the location where minimum OLR was encountered ranged from 793 km in the southern tropical Andes to 1208 km in the northern tropical Andes (Figure 10c). In JJA, there were more than 1500 km between the measurement location and the location where minimum OLR was encountered in the tropical Andes and more than 2000 km in the northern subtropical Andes (Figure 10d). Average regional OLR at the time of trajectory initiation was 261 W m^{-2} and 265 W m^{-2} in DJF and JJA, respectively. These results suggest that local convection does not exert a primary control over δD_{vapor} or $\Delta\delta D$ in either austral summer or austral winter.

4. Discussion

There is a significant negative correlation ($r = -0.40$, $p < 0.0001$) between $\Delta\delta D$ and minimum OLR along back trajectories, suggesting that δD_{vapor} that falls below the Rayleigh curve is associated with intense upwind convection during DJF. Positive $\Delta\delta D$ values are generally associated with mesoscale, organized convective systems upwind of the measuring site rather than local storms [e.g., *Lawrence et al.*, 2004]. There are two main mechanisms proposed for decreasing the δD_{vapor} in convective storms: low saturation temperatures in high cumulonimbus clouds [e.g., *Lawrence*, 2003; *Thompson et al.*, 2003] or increased entrainment of low δD water vapor from the unsaturated downdraft into the subcloud layer that feeds the convective system and diffusive exchanges [e.g., *Risi et al.*, 2008].

It is difficult to directly evaluate the influence of low saturation temperatures on the isotopic composition of water vapor measured over the tropical Andes. Cloud top temperature data are available, but previous studies have shown that water vapor typically condenses at lower altitudes and higher temperatures than the top of the cloud during convective storms [e.g., *Smith*, 1992]. It is, therefore, impossible to directly evaluate saturation temperatures without echo top data [e.g., *Scholl et al.*, 2009], which can be obscured by high clouds in the tropics [*Riley and Mapes*, 2009]. Models indicate that condensation altitude and temperature variations play no role in the decreased δD_{vapor} associated with the amount effect [*Risi et al.*, 2008]. More significant factors include the decreased isotopic composition of subcloud layer vapor with increased entrainment of low δD water vapor from the unsaturated downdraft [e.g., *Risi et al.*, 2008] and converged water vapor [e.g., *Moore et al.*, 2014] along with diffusive exchanges, which become more efficient at high relative humidity [e.g., *Dansgaard*, 1964; *Risi et al.*, 2008]. Therefore, relatively low DJF δD_{vapor} likely records upwind convective intensity, most likely associated with the South American summer monsoon, rather than atmospheric temperature. This is consistent with the Andean Isotope Index [*Hoffmann*, 2003], precipitation studies from the northern and southern tropical Andes [*Vimeux et al.*, 2005; *Villacís et al.*, 2008], and models [*Vuille et al.*, 2003a; *Vimeux et al.*, 2009].

The majority of JJA TES measurements have negative $\Delta\delta D$ values. Processes that produce this relationship between q and δD_{vapor} include large-scale advective mixing [*Dessler and Sherwood*, 2003; *Noone*, 2012] and ice lofting with subsequent sublimation in convective clouds [e.g., *Smith*, 1992]. JJA δD_{vapor} generally falls on a mixing curve. Although mixing can occur between any number of air parcels last saturated in different regions [*Galewsky and Hurley*, 2010], we can simplify the process into a simple two-component mixing model. The curve that best describes the data has a moist end-member with $q = 19162$ ppmv and $\delta D_{vapor} = -86$‰ and a dry end-member with $q = 574$ ppmv and $\delta D_{vapor} = -496$‰ (Figure 2b). The moist end-member may itself be the product of mixing between marine boundary layer air and recycled moisture from the Amazon Basin. The dry end-member has an isotopic composition consistent with water vapor in the upper tropical troposphere [e.g., *Bony et al.*, 2008; *Blossey et al.*, 2010] and may represent subsidence of air dehydrated via convection [e.g., *Galewsky et al.*, 2011] in the ITCZ, which lies to the north of the equator in JJA.

5. Conclusions

Our goal was to investigate the relationship between water vapor isotopic ratios and upwind convection in the tropical and northern subtropical Andes in order to improve our understanding of large-scale water vapor dynamics that, ultimately, deliver moisture to tropical glaciers. Specifically, this study shows that

1. Average δD_{vapor} in the tropical Andes is 13‰ to 43‰ lower in austral summer than austral winter despite relatively uniform annual air temperatures.
2. δD_{vapor} is, on average, 18‰ to 36‰ lower than predicted by the Rayleigh model in the tropical Andes in austral summer and 6‰ to 142‰ above the Rayleigh curve in austral winter.

3. δD is higher than predicted by Rayleigh fractionation (i.e., $\Delta\delta D > 0‰$) for more than half of the DJF TES δD_{vapor} measurements but for only ~40% of the JJA TES measurements.
4. More than 90% of positive $\Delta\delta D$ measurements in DJF have minimum upwind OLR $< 240\,W\,m^{-2}$ (high convective intensity), and all of the measurements with positive $\Delta\delta D$ encountered lower minimum upwind OLR than measurements with negative $\Delta\delta D$ regardless of season.

Previous studies have linked upwind convection to lower δD_{vapor} than predicted by the Rayleigh model at the given q [e.g., *Noone*, 2012] and to $\delta^{18}O_{snow}$ in the tropical Andes [e.g., *Vimeux et al.*, 2005; *Villacís et al.*, 2008]. The regional coverage of the satellite data allows us to explore this link between low isotopic ratios and upwind convection and to examine the spatial extent of the region where convection controls isotopic ratios of water vapor. TES measurements with positive $\Delta\delta D$ in DJF are centered in the central tropical Andes and to the east of the central tropical Andes in the area affected by the South American summer monsoon. The JJA measurements with $\Delta\delta D > 0‰$ are north of the tropical Andes and north of the equator. This result suggests that deep convection associated with the South American summer monsoon controls δD_{vapor} in DJF while convection in the ITCZ controls a small proportion of the relatively low δD_{vapor} in austral winter.

Pacific sea surface temperature (SST) and SST anomalies associated with the El Niño–Southern Oscillation strongly influence convective intensity upwind of the glaciers by controlling the position of the ITCZ, strength of the Hadley Circulation, Atlantic SST variations [*Wang*, 2004], South American precipitation [*Lenters and Cook*, 1999], and Altiplano climate [*Vuille et al.*, 2000]. Modeling studies and studies based on reconstructed SST have linked isotopic profiles through tropical Andean ice cores to both Pacific SST and SST anomalies [*Henderson et al.*, 1999; *Vuille et al.*, 2003a; *Thompson et al.*, 2013]. Overall, our results, based on satellite observations, are consistent with modeling studies [*Vuille et al.*, 2003b] and with studies based on individual glaciers [*Hardy*, 2003; *Vimeux et al.*, 2005; *Villacís et al.*, 2008] and suggest that tropical convection, rather than temperature, exerts a primary control over $\delta^{18}O_{snow}$ in the tropical Andes.

Acknowledgments

Part of this research was carried out at the Jet Propulsion Laboratory, California Institute of Technology, under a contract with the National Aeronautics and Space Administration. AIRS data were obtained from the Mirador online database, developed and maintained by GES DISC. The authors gratefully acknowledge the NOAA Air Resources Laboratory (ARL) for the provision of the HYSPLIT transport and dispersion model. Thanks to Vicencio Expeditions for making field work at Quelccaya both possible and pleasant. We thank three anonymous reviewers for their constructive suggestions. Funding for Samuels-Crow was provided by NM EPSCoR.

References

Blossey, P. N., Z. Kuang, and D. M. Romps (2010), Isotopic composition of water in the tropical tropopause layer in cloud-resolving simulations of an idealized tropical circulation, *J. Geophys. Res.*, *115*, D24309, doi:10.1029/2010JD014554.

Bony, S., C. Risi, and F. Vimeux (2008), Influence of convective processes on the isotopic composition (δ18O and δD) of precipitation and water vapor in the tropics: 1. Radiative-convective equilibrium and Tropical Ocean–Global Atmosphere–Coupled Ocean-Atmosphere Response Experiment (TOGA-COARE) simulations, *J. Geophys. Res.*, *113*, D19305, doi:10.1029/2008JD009942.

Bradley, R. S., F. T. Keimig, H. F. Diaz, and D. R. Hardy (2009), Recent changes in freezing level heights in the Tropics with implications for the deglacierization of high mountain regions, *Geophys. Res. Lett.*, *36*, L17701, doi:10.1029/2009GL037712.

Broecker, W. (1997), Mountain glaciers: Recorders of atmospheric water vapor content?, *Global Biogeochem. Cycles*, *11*(4), 589–597, doi:10.1029/97GB02267.

Brown, D., J. Worden, and D. Noone (2008), Comparison of atmospheric hydrology over convective continental regions using water vapor isotope measurements from space, *J. Geophys. Res.*, *113*, D15124, doi:10.1029/2007JD009676.

Craig, H., and L. Gordon (1965), in *Deuterium and Oxygen 18 Variations in the Ocean and the Marine Atmosphere*, edited by E. Tongiorgi, Laboratorio de Geologia Nucleare, Pisa.

Dansgaard, W. (1964), Stable isotopes in precipitation, *Tellus*, *16*(4), 436–468.

Dessler, A., and S. Sherwood (2003), A model of HDO in the tropical tropopause layer, *Atmos. Chem. Phys. Discuss.*, *3*(4), 4489–4513.

Draxler, R. R. (1999), HYSPLIT4 user's guide. NOAA Tech. Memo. ERL ARL-230, NOAA Air Resources Laboratory, Silver Spring, Md., 38 pp.

Draxler, R. R., and G. D. Hess (1997), Description of the HYSPLIT_4 modeling system. NOAA Tech. Memo. ERL ARL-224, NOAA Air Resources Laboratory, Silver Spring, Md., 24 pp.

Friedman, I. (1953), Deuterium content of natural waters and other substances, *Geochim. Cosmochim. Acta*, *4*(1–2), 89–103.

Galewsky, J., and J. V. Hurley (2010), An advection-condensation model for subtropical water vapor isotopic ratios, *J. Geophys. Res.*, *115*, D16116, doi:10.1029/2009JD013651.

Galewsky, J., C. Rella, Z. Sharp, K. Samuels, and D. Ward (2011), Surface measurements of upper tropospheric water vapor isotopic composition on the Chajnantor Plateau, Chile, *Geophys. Res. Lett.*, *38*, L17803, doi:10.1029/2011GL048557.

Garreaud, R., M. Vuille, and A. C. Clement (2003), The climate of the altiplano: Observed current conditions and mechanisms of past changes, *Palaeogeogr. Palaeoclimatol. Palaeoecol.*, *194*(1–3), 5–22, doi:10.1016/S0031-0182(03)00269-4.

Garreaud, R. D., M. Vuille, R. Compagnucci, and J. Marengo (2008), Present-day South American climate, *Palaeogeogr. Palaeoclimatol. Palaeoecol.*, *281*, 180–195, doi:10.1016/j.palaeo.2007.10.032.

Gat, J. (1996), Oxygen and hydrogen isotopes in the hydrologic cycle, *Annu. Rev. Earth Planet Sci.*, *24*(1), 225–262.

Gedzelman, S. D. (1988), Deuterium in water vapor above the atmospheric boundary layer, *Tellus B*, *40*(2), 134–147.

Grootes, P., M. Stuiver, L. Thompson, and E. Mosley-Thompson (1989), Oxygen isotope changes in tropical ice, Quelccaya, Peru, *J. Geophys. Res.*, *94*(D1), 1187–1194, doi:10.1029/JD094iD01p01187.

Hardy, D. R. (2011), High-elevation weather stations on glaciers in the Tropics 2011 update, in *Workshop on the use of Automatic Measuring Systems on Glaciers*, edited by C. H. Tijm-Reijmer and J. Oerlemans, pp. 45–48, Institute for Marine and Atmospheric Research Utrecht, Utrecht Univ., Pontresina, Switzerland.

Hardy, D. R., and S. P. Hardy (2008), White-winged Diuca Finch (Diuca speculifera) nesting on Quelccaya Ice Cap, Perú, *Wilson J. Ornithol.*, *120*(3), 613–617.

Hardy, D. R., M. Vuille, and R. S. Bradley (2003), Variability of snow accumulation and isotopic composition on Nevado Sajama, Bolivia, *J. Geophys. Res.*, *108*(D22), 4693, doi:10.1029/2003JD003623.
Henderson, K. A., L. G. Thompson, and P. N. Lin (1999), Recording of El Niño in ice core δ18O records from Nevado Huascarán, Peru, *J. Geophys. Res.*, *104*(D24), 31,053–31,065, doi:10.1029/1999JD900966.
Hoffmann, G., et al. (2003), Coherent isotope history of Andean ice cores over the last century, *Geophys. Res. Lett.*, *30*(4), 1179, doi:10.1029/2002GL014870.
Johnson, L. R., Z. D. Sharp, J. Galewsky, M. Strong, A. D. Van Pelt, F. Dong, and D. Noone (2011), Hydrogen isotope correction for laser instrument measurement bias at low water vapor concentration using conventional isotope analyses: Application to measurements from Mauna Loa Observatory, Hawaii, *Rapid Commun. Mass Spectrom.*, *25*(5), 608–616, doi:10.1002/rcm.4894.
Kaser, G., and H. Osmaston (2002), *Tropical Glaciers*, Cambridge Univ. Press, Cambridge.
Kousky, V. E. (1988), Pentad outgoing longwave radiation climatology for the South American sector, *Rev. Bras. Meteorol.*, *3*(1), 217–231.
Kousky, V. E., and M. T. Kayano (1994), Principal modes of outgoing longwave radiation and 250-mb circulation for the South American sector, *J. Clim.*, *7*(7), 1131–1143.
Lacour, J. L., C. Risi, L. Clarisse, S. Bony, D. Hurtmans, C. Clerbaux, and P. F. Coheur (2012), Mid-tropospheric δD observations from IASI/MetOp at high spatial and temporal resolution, *Atmos. Chem. Phys.*, *12*(22), 10,817–10,832, doi:10.5194/acp-12-10817-2012.
Lawrence, J. R. (2003), Tropical ice core isotopes: Do they reflect changes in storm activity?, *Geophys. Res. Lett.*, *30*(2), 1072, doi:10.1029/2002GL015906.
Lawrence, J. R., S. D. Gedzelman, D. Dexheimer, H. K. Cho, G. D. Carrie, R. Gasparini, C. R. Anderson, K. P. Bowman, and M. I. Biggerstaff (2004), Stable isotopic composition of water vapor in the tropics, *J. Geophys. Res.*, *109*, D06115, doi:10.1029/2003JD004046.
Lee, J., J. Worden, D. Noone, K. Bowman, A. Eldering, A. LeGrande, J. L. F. Li, G. Schmidt, and H. Sodemann (2011), Relating tropical ocean clouds to moist processes using water vapor isotope measurements, *Atmos. Chem. Phys.*, *11*(2), 741–752, doi:10.5194/acp-11-741-2011.
Lenters, J. D., and K. H. Cook (1999), Summertime precipitation variability over South America: Role of the large-scale circulation, *Mon. Weather Rev.*, *127*(3), 409–431, doi:10.1175/1520-0493(1999)127<0409:SPVOSA>2.0.CO;2.
Majoube, M. (1971), Oxygen-18 and deuterium fractionation between water and steam, *J. Chim. Phys. Physicochim. Biol.*, *68*, 1423–1436.
Martínez, R., D. Ruiz, M. Andrade, L. Blacutt, and D. Pabón (2011), Synthesis of the Climate of the Tropical Andes, in *Climate Change and Biodiversity in the Tropical Andes*, edited by S. K. Herzog et al., pp. 97–109, Inter-American Institute of Global Change Research (IAI) and Scientific Committee on Problems of the Environment (SCOPE), São José dos Campos, Brazil.
Merlivat, L., and G. Nief (1967), Fractionnement isotopique lors des changements d "état solide-vapeur et liquide-vapeur de l"eau à des températures inférieures à 0° C, *Tellus*, *19*, 122–127.
Moore, M., Z. Kuang, and P. N. Blossey (2014), A moisture budget perspective of the amount effect, *Geophys. Res. Lett.*, *41*, 1329–1335, doi:10.1002/2013GL058302.
Moron, V. (1995), Variability of the African convection centre as viewed by outgoing longwave radiation records and relationships with sea-surface temperature patterns, *Int. J. Climatol.*, *15*(1), 25–34.
Noone, D. (2012), Pairing measurements of the water vapor isotope ratio with humidity to deduce atmospheric moistening and dehydration in the tropical midtroposphere, *J. Clim.*, *25*(13), 4476–4494, doi:10.1175/JCLI-D-11-00582.1.
Pierrehumbert, R. (1999), Huascaran δ18O as an indicator of tropical climate during the Last Glacial Maximum, *Geophys. Res. Lett.*, *26*(9), 1345–1348, doi:10.1029/1999GL900183.
Ramirez, E., et al. (2003), A new Andean deep ice core from Nevado Illimani (6350 m), Bolivia, *Earth Planet. Sci. Lett.*, *212*(3–4), 337–350, doi:10.1016/S0012-821X(03)00240-1.
Riley, E. M., and B. E. Mapes (2009), Unexpected peak near −15°C in CloudSat echo top climatology, *Geophys. Res. Lett.*, *36*, L09819, doi:10.1029/2009GL037558.
Risi, C., S. Bony, and F. Vimeux (2008), Influence of convective processes on the isotopic composition (δ18O and δD) of precipitation and water vapor in the tropics: 2. Physical interpretation of the amount effect, *J. Geophys. Res.*, *113*, D19306, doi:10.1029/2008JD009943.
Risi, C., S. Bony, F. Vimeux, C. Frankenberg, D. Noone, and J. Worden (2010), Understanding the Sahelian water budget through the isotopic composition of water vapor and precipitation, *J. Geophys. Res.*, *115*, D24110, doi:10.1029/2010JD014690.
Scholl, M. A., J. B. Shanley, J. P. Zegarra, and T. B. Coplen (2009), The stable isotope amount effect: New insights from NEXRAD echo tops, Luquillo Mountains, Puerto Rico, *Water Resour. Res.*, *45*, W12407, doi:10.1029/2008WR007515.
Singh, C. V. (2005), Principal component analysis of satellite-observed outgoing long-wave radiation during the monsoon period (June–September) over India, *Theor. Appl. Climatol.*, *84*(4), 207–211, doi:10.1007/s00704-005-0170-z.
Smith, G. (1992), Deuterium in North-Atlantic storm tops, *J. Atmos. Sci.*, *49*(22), 2041–2057.
Strong, M., Z. D. Sharp, and D. S. Gutzler (2007), Diagnosing moisture transport using D/H ratios of water vapor, *Geophys. Res. Lett.*, *34*, L03404, doi:10.1029/2006GL028307.
Sturm, C., F. Vimeux, and G. Krinner (2007), Intraseasonal variability in South America recorded in stable water isotopes, *J. Geophys. Res.*, *112*, D20118, doi:10.1029/2006JD008298.
Susskind, J., G. Molnar, L. Iredell, and N. G. Loeb (2012), Interannual variability of outgoing longwave radiation as observed by AIRS and CERES, *J. Geophys. Res.*, *117*, D23107, doi:10.1029/2012JD017997.
Thompson, L. (2000), Ice core evidence for climate change in the Tropics: Implications for our future, *Quat. Sci. Rev.*, *19*(1–5), 19–35.
Thompson, L., E. Mosley-Thompson, and K. Henderson (2000), Ice-core palaeoclimate records in tropical South America since the Last Glacial Maximum, *J. Quaternary Sci.*, *15*(4), 377–394.
Thompson, L. G., E. Mosley-Thompson, M. E. Davis, P. N. Lin, K. A. Henderson, J. Cole-Dai, J. F. Bolzan, and K.-B. Liu (1995), Late glacial stage and Holocene tropical ice core records from Huascaran, Peru, *Science*, *269*(5220), 46–50.
Thompson, L., E. Mosley-Thompson, M. Davis, P. Lin, K. Henderson, and T. Mashiotta (2003), Tropical glacier and ice core evidence of climate change on annual to millennial time scales, *Clim. Change*, *59*(1), 137–155.
Thompson, L. G., E. Mosley-Thompson, M. Davis, V. S. Zagordnov, M. Howat, V. N. Mikhalenko, and P. N. Lin (2013), Annually resolved Ice core records of tropical climate variability over the past ~1800 years, *Sci. Express*, *340*, 945–950, doi:10.1126/science.1234210.
Villacís, M., F. Vimeux, and J. D. Taupin (2008), Analysis of the climate controls on the isotopic composition of precipitation (δ18O) at Nuevo Rocafuerte, 74.5°W, 0.9°S, 250 m, Ecuador, *C. R. Geosci.*, *340*(1), 1–9, doi:10.1016/j.crte.2007.11.003.
Vimeux, F., R. Gallaire, S. Bony, G. Hoffmann, and J. Chiang (2005), What are the climate controls on δD in precipitation in the Zongo Valley (Bolivia)? Implications for the Illimani ice core interpretation, *Earth Planet. Sci. Lett.*, *240*(2), 205–220, doi:10.1016/j.epsl.2005.09.031.
Vimeux, F., P. Ginot, M. Schwikowski, M. Vuille, G. Hoffmann, L. G. Thompson, and U. Schotterer (2009), Climate variability during the last 1000 years inferred from Andean ice cores: A review of methodology and recent results, *Palaeogeogr. Palaeoclimatol. Palaeoecol.*, *281*(3–4), 229–241, doi:10.1016/j.palaeo.2008.03.054.

Vimeux, F., G. Tremoy, C. Risi, and R. Gallaire (2011), Earth and Planetary Science Letters, *Earth Planet. Sci. Lett.*, *307*(1–2), 47–58, doi:10.1016/j.epsl.2011.04.031.

Vuille, M., and M. Werner (2005), Stable isotopes in precipitation recording South American summer monsoon and ENSO variability: Observations and model results, *Clim. Dyn.*, *25*(4), 401–413, doi:10.1007/s00382-005-0049-9.

Vuille, M., R. S. Bradley, and F. Keimig (2000), Interannual climate variability in the Central Andes and its relation to tropical Pacific and Atlantic forcing, *J. Geophys. Res.*, *105*(D10), 12,447–12,460, doi:10.1029/2000JD900134.

Vuille, M., R. Bradley, R. Healy, M. Werner, D. Hardy, L. Thompson, and F. Keimig (2003a), Modeling delta O-18 in precipitation over the tropical Americas: 2. Simulation of the stable isotope signal in Andean ice cores, *J. Geophys. Res.*, *108*(D6), 4175, doi:10.1029/2001JD002039.

Vuille, M., R. S. Bradley, M. Werner, and F. Keimig (2003b), 20th century climate change in the tropical Andes: Observations and model results, *Clim. Change*, *59*(1), 75–99.

Wang, C. (2004), ENSO, Atlantic climate variability, and the Walker and Hadley circulations, in *The Hadley Circulation: Present, Past, and Future*, Adv. Global Change Res., vol. 21, edited by H. F. Diaz and R. S. Bradley, pp. 173–202, Springer, Netherlands.

Windhorst, D., T. Waltz, E. Timbe, H. G. Frede, and L. Breuer (2013), Impact of elevation and weather patterns on the isotopic composition of precipitation in a tropical montane rainforest, *Hydrol. Earth Syst. Sci.*, *17*(1), 409–419, doi:10.5194/hess-17-409-2013.

Worden, J., et al. (2006), Tropospheric Emission Spectrometer observations of the tropospheric HDO/H 2O ratio: Estimation approach and characterization, *J. Geophys. Res.*, *111*, D16309, doi:10.1029/2005JD006606.

Worden, J., et al. (2007), Importance of rain evaporation and continental convection in the tropical water cycle, *Nature*, *445*(7127), 528–532, doi:10.1038/nature05508.

Worden, J., S. Kulawik, C. Frankenberg, V. Payne, K. Bowman, K. Cady-Peirara, K. Wecht, J. E. Lee, and D. Noone (2012), Profiles of CH_4, HDO, H_2O, and N_2O with improved lower tropospheric vertical resolution from Aura TES radiances, *Atmos. Meas. Tech.*, *5*(2), 397–411, doi:10.5194/amt-5-397-2012.

Zhang, C. (1993), Large-scale variability of atmospheric deep convection in relation to sea surface temperature in the tropics, *J. Clim.*, *6*(10), 1898–1913.

Zhou, J., and K. M. Lau (1998), Does a monsoon climate exist over South America?, *J. Clim.*, *11*(5), 1020–1040.